Environmental Science and Pollution Research (2022) 29:41505–41519
https://doi.org/10.1007/s11356-021-18263-y

RESEARCH ARTICLE

CuO nanoparticles decorated on hydroxyapatite/ferrite magnetic support: photocatalysis, cytotoxicity, and antimicrobial response

Elaine Cristina Paris[1] · João Otávio Donizette Malafatti[1,2] · Ailton José Moreira[2] · Lílian Cruz Santos[1,2] · Camila Rodrigues Sciena[1,2] · Alessandra Zenatti[3] · Márcia Tsuyama Escote[3] · Valmor Roberto Mastelaro[4] · Miryam Rincón Joya[5]

Received: 27 May 2021 / Accepted: 17 December 2021 / Published online: 28 January 2022

Abstract

Photocatalysts supported in magnetic nanocomposites for application in environmental remediation processes have been evaluated for removing contaminants due to easy recovery and low toxicity to the ecosystem. In this work, copper oxide (CuO) nanoparticles with photocatalytic properties were decorated on magnetic support constituted by hydroxyapatite (HAP) and ferrite to achieve efficiency in contaminated water remediation under visible light irradiation. First, nanomaterials were obtained by precipitation route, allowing fast and straightforward synthesis. Then, CuO nanoparticles with 6 nm diameter were efficiently decorated on magnetic support (25 nm), showing a high ability to absorb visible light irradiation (bandgap) to promote electronic transition and charge separation. Under visible irradiation, CuO promotes the H_2O_2 reduction in the conduction band (BC) to form hydroxyl radicals ($^{\bullet}OH$), which are responsible for rhodamine B (RhB) dye degradation (> 90% in 60 min). Magnetic hysteresis assays confirmed the magnetic properties of HAP/ferrite support, which enabled the recovery and reuse of the magnetic photocatalyst efficiently up to 3 cycles. Due to low Cu^{2+} leaching after the photocatalytic application stage, cytotoxicity assay for the *Allium cepa* seeds did not exhibit abnormal cells other than those commonly found. Furthermore, the CuO-decorated nanoparticles showed bactericidal activity against *S. aureus* (Gram-positive) and *E. coli* (Gram-negative) microorganisms, being more significant for the first one. Thus, the developed nanocomposite of CuO nanoparticles decorated on the magnetic support surface showed to be a complete system for water remediation, acting in contaminant degradation under visible light irradiation and bactericidal control with environmentally friendly characteristics.

Keywords Copper oxide · Magnetic nanocomposite · Photocatalyst · Cytotoxicity · Bactericidal

Responsible Editor: Sami Rtimi

✉ Elaine Cristina Paris
elaine.paris@embrapa.br

[1] Nanotechnology National Laboratory for Agriculture (LNNA), Embrapa Instrumentação, XV de Novembro St., 1452, São Carlos, SP 13560-970, Brazil

[2] Department of Chemistry, Federal University of São Carlos, Rod. Washington Luiz, km 235, zip code: 13565-905, São Carlos, SP, Brazil

[3] Center for Engineering, Modeling, and Applied Social Sciences, Federal University of ABC, Avenida dos Estados, 5001, Santo André, SP 09210-580, Brazil

[4] São Carlos Institute of Physics, University of São Paulo, São Carlos, SP 13566-590120, Brazil

[5] Departamento de Física, Facultad de Ciencias, Universidad Nacional de Colombia-Bogota, Carrera 30 Calle 45-03, 111321 Bogota, Colombia

Introduction

The issues of pollution and environmental preservation have attracted scientific attention to developing alternative methods for effluent remediation (Xue et al. 2017). In this context, advanced oxidative processes (AOPs) are in evidence due to the capability of mineralizing the organic pollutants to inorganic compounds, such as CO_2 and H_2O (Sharma et al. 2019). Heterogeneous photocatalysis is a branch of AOPs that uses semiconductors and light energy to generate oxidative species responsible for pollutant mineralization (Mageshwari et al. 2015). Semiconductors such as TiO_2 (Pedrosa et al. 2018; Moreira et al. 2020b), SnO (Hu et al. 2017), ZnO (Shinde et al. 2017; Ruellas et al. 2019), Nb_2O_5 (Malafatti et al. 2020), and CuO (Raba-Páez et al. 2020a) have been applied with success in photocatalytic degradation of drugs, pesticides, and dyes. CuO stands out among these

oxides due to its bandgap range of the visible spectrum, stability, and low cost (Raba-Páez et al. 2020b). Meshram and collaborators (Meshram et al. 2012) synthesized CuO nanoparticles with different forms altering synthesis parameters. They observed that the plate form was the most effective in the methylene blue degradation under sunlight. CuO is a p-type semiconductor, stable, and a prominent photocatalyst to promote oxidation reactions in the valence band aiming at the formation of reactive oxygen species (Raba-Páez et al. 2020a). Another property that optimizes CuO's ability to photocatalyze chemical reactions is the hydrophobicity, which in the H_2O_2 presence can be increased due to oxidation processes (Tu et al. 2014). In addition, photocatalysts with evident hydrophilicity have promoted more significant interaction between the material and pollutant molecule in the aqueous medium, increasing the photocatalytic reaction efficiency (Osman et al. 2017; Ghashghaee et al. 2019). Due to these properties, CuO has been applied in anode cells of lithium-ion batteries (Xiang et al. 2010), in supercapacitors (Wang et al. 2014), catalysts (Bordbar et al. 2017; Rana and Jonnalagadda 2017), photocatalysts (Novikova et al. 2016), and gas sensors (Li et al. 2019). CuO is an antimicrobial agent for fungi, bacteria, and viruses (Gallo et al. 2018; Tavakoli and Hashemzadeh 2020), which significantly increases the potential for technological applications. CuO can be obtained in different nanoparticle forms according to synthetic methodologies, such as sol–gel (Usha et al. 2015), hydrothermal (Jiang et al. 2014), controlled precipitation (Phiwdang et al. 2013), instantaneous precipitation (Ahamed et al. 2014), combustion (Dong et al. 2015), and microwave-hydrothermal (Moura et al. 2010).

Heterogeneous photocatalysis is a promising technique that has been exploited to become increasingly sustainable and environmentally friendly. Recent studies have obtained photocatalysts through industrial waste (Augusto et al. 2018; Osman et al. 2020), allowing the circular economy to integrate the list of advantages of heterogeneous photocatalysis. However, the photocatalyst application still has limitations due to the material development with properties that allow the adoption of efficient methodologies for removal after the application stage. Thus, magnetic nanocomposites have been an alternative to promote a simple separation and reuse in new cycles in the remediation process (Zhao et al. 2015).

The magnetic nanoparticles have been evaluated as support due to using a magnetic field for photocatalyst recovering (Paris et al. 2020c). The magnetic nanoparticles most used as support of active compounds are magnetite (Fe_3O_4) (Hamzezadeh-Nakhjavani et al. 2015), greigite (Fe_3S_4) (Yang et al. 2018), maghemite (γ-Fe_2O_3) (Rincón Joya et al. 2019), and general ferrites ($MeFe_2O_4$), where Me = Co, Mg, Ni, Fe, Ni, Mn, and others (Paris et al. 2020a). However, some challenges need to be met for the efficient use of magnetic supports. The main one is to avoid the agglomerate formations resulting from magnetic spin alignment (Nolting et al. 2000; Paris et al. 2020b). Consequently, the agglomeration promotes a decrease in the active material surface area anchored to the support surface. One way to minimize this harmful effect is by anchoring magnetic particles in porous support, such as HAP (Coutinho et al. 2018), zeolite (Zhao et al. 2015), and silica (Harraz et al. 2014), allowing the magnetic material dispersion and stability.

HAP is a promisor bioceramic widely applied to medical and pharmaceutics materials, sensor array, adsorption, and catalysis due to the biocompatibility, high porosity, and accessible surface modification (André et al. 2012; Pereira et al. 2017; Coutinho et al. 2018). Materials based on HAP and ferrite magnetic nanoparticles have significantly improved nanocomposites' magnetic properties and biocompatibility, becoming an alternative to environmental remediation involving heterogeneous photocatalysis (Valizadeh et al. 2014; Ain et al. 2020). However, as far as it is known, no study has been found regarding the literature about CuO nanoparticles supported on HAP/ferrite porous magnetic nanocomposite. Thus, this work aims to evaluate the CuO nanoparticle decoration on HAP/ferrite magnetic support to verify the maintenance of the CuO photocatalyst properties aiming to RhB dye photodegradation under visible light irradiation. Furthermore, the nanocomposite was evaluated as a potential antimicrobial agent against *S. aureus* (Gram-positive) and *E. coli* (Gram-negative) bacteria models. Finally, the magnetic properties and cytotoxicity effect in plants were investigated to elucidate the photocatalyst system recovery and stability capacity for reuse in new cycles to minimize environmental damage.

Materials and methods

Synthesis

CuO nanoparticles

The cupric oxide nanoparticle synthesis route was based on the methodology presented by Zhu et al. (2008). In the synthesis procedure, 0.03 M of copper acetate (Synth) as a precursor to Cu^{2+} ions was solubilized in 300 mL of water. In sequence, 1 mL of glacial acetic acid was added, and the temperature increased until the boiling point. After adding 0.1 M sodium hydroxide (Synth) pellets, a black precipitate was formed instantaneously. Then, the reaction medium was cooled until room temperature. Finally, the precipitate was washed until pH 7 and subsequently dried at 60 °C in a circulation oven.

HAP/ferrite magnetic support

HAP support and iron ferrite (HAP/ferrite) was synthesized by chemical precipitation based on Yang et al. (2010). Previously, in 30 mL of deionized water was added an N_2 flow for 10 min, maintained throughout the experimental procedure. Next, the Fe^{2+} and Fe^{3+} precursor ions were added by 1.85 mmol of $FeCl_2.4\ H_2O$ (Sigma-Aldrich) and 3.7 mmol of $FeCl_3.6\ H_2O$ (Sigma-Aldrich) under stirring until obtaining a homogeneous solution. Posteriorly, 10 mL of the mineralizing agent NH_4OH (32%, Synth) was dripped and heated until 80 °C for 30 min. Next, a citric acid solution (0.1 M) was added to the reaction medium, and the temperature was raised to 90 °C for 1.5 h. Finally, the black precipitate was washed with N_2 purged water at neutral pH and dried at 60 °C in an air circulation oven. In order to prepare the 1:1 (w/w) HAP/ferrite magnetic support, the ferrite was dispersed in 50 mL of water, containing 33.7 mmol of the HAP precursor $Ca(NO_3)_2.4\ H_2O$ (Vetec) under N_2 flow. The pH 11 was maintained (NH_4OH) during all procedures. Then, 20 mmol of $(NH_4)_2HPO_4$ (Synth) was dropped onto the solution, resulting in the HAP and ferrite composite. Next, the suspension containing the precipitated was heated to 90 °C and maintained at this temperature for 2 h. In sequence, the dispersion was cooled, centrifuged, and washed with deionized water (CO_2-free) to neutral pH and dried in an air circulation oven at 60 °C.

CuO immobilization on HAP/ferrite

CuO immobilization on the porous magnetic support HAP/ferrite surface was performed using high-intensity ultrasound (Branson Digital Sonifier). The nanocomposite was obtained in the 3:1 (w/w) by 80 mg of the magnetic ferrite and 20 mg of the CuO nanoparticles in 50 mL of deionized water. First, the mixture was under ultrasound tip (30% frequency) in an ice bath for 1 h. Then, the dispersion was centrifuged and dried at 60 °C in an air circulation oven.

Characterization

X-ray diffraction (XRD) measurements were performed on a Shimadzu XRD 6000 diffractometer, using Cu Kα radiation ($\lambda = 1.5406$ Å). The operation voltage and current were maintained at 30 kV and 30 mA, respectively. The sample morphologies were evaluated using the JEOL JMS 6701F equipment in a field emission microscope (FEG-SEM), operating at current extraction voltages of 2 to 10 kV. The transmission electron microscopy (TEM) was realized in an FEI Tecnai F20 G2 HRTEM. The zeta potential was measured using a zeta potential meter (Malvern Zetasizer nano-Zs model). The specific surface areas were measured by nitrogen adsorption at 77 K (Micromeritics ASAP-2020) and calculated by the Brunauer–Emmett–Teller (BET) method. The elemental composition distributions of magnetic nanocomposites were evaluated using energy dispersive spectroscopy (EDS) coupled to the scanning electron microscope (SEM, JEOL 6510) in a 6742[a] model spectrometer with UltraDry Silicon Drift Detector (SDD) and resolution of 132 eV. The magnetic measurements were performed using an optical magnetizer (PPMS), PPMS 9 Evercool, Quantum Design model, India. The parameters used were the zero-field-cooled (ZFC) and field-cooled (FC) protocoled, external field applied of 100 Oe at room temperature in a range of − 20,000 to 200,000 Oe. Diffuse reflectance spectra (DRS) in the ultraviolet–visible (UV–vis) region were recorded at room temperature between 200 and 1200 nm using a spectrometer (Shimadzu, Japan). Thus, the bandgap energy was obtained by applying the Kubelka–Munk model. The surface chemical analysis of the samples was performed by X-ray photoelectron spectroscopy (XPS), using a conventional XPS spectrometer (Scienta Omicron ESCA +) with a 128-channel hemispheric analyzer (EAC2000) and Al Kα monochromatic radiation ($h\nu = 1486.6$ eV) as the excitation source. The high-resolution XPS spectra were recorded at constant pass energy of 20 eV with 0.05 eV per step. During the measurements, a charge neutralizer was used to prevent the samples from electrically charging. The XPS spectra were calibrated by the C 1 s peak with the binding energy around 284.8 eV and analyzed using the Casa-XPS software.

Photocatalytic assay

Photocatalytic assays of CuO-free nanoparticles and supported on HAP/ferrite surface were performed in a 20 mL aqueous solution containing RhB dye (5 mg L^{-1}). Previously, the adsorption/desorption processes were realized for 12 h at 20 °C in the dark. The CuO-free photocatalytic activity was initially available under different hydrogen peroxide (H_2O_2) volumes (0.1, 0.2, 0.5, 1.0, 1.5, and 2.0 mL) and variable CuO concentrations (50, 75, 100, and 150 mg L^{-1}) in order to determine the optimized condition of RhB photodegradation under visible light irradiation. Then, using a thermostatic photoreactor, CuO immobilized on HAP/ferrite magnetic support was applied in RhB photocatalysis at different exposition times to light source. After the exposition, the CuO/HAP/ferrite nanocomposite was separated by magnetic removal, washed, and reused in new cycles. The results were analyzed by UV–vis spectroscopy between the 800 and 200 nm spectrum range. Probe assays for $^{\bullet}OH$ were performed following the procedure described in the literature (Malafatti et al. 2020). Thus, 10 mL of a 1.5 mg L^{-1} coumarin (COU) solution (99%, Sigma-Aldrich) was added in a 50-mL beaker in the presence of 2.0 mL of H_2O_2

(35% V V^{-1}) and 100 mg L^{-1} of the CuO photocatalysts or CuO/HAP/ferrite. The different samples were irradiated under visible light for 2 h and then filtered with a 0.45 µm membrane to remove the catalysts. The reaction product was analyzed by photoluminescence (PL) spectroscopy for •OH formation monitoring. In order to determine the radiation spectra emitted by the photoreactor, a spectroradiometer SPR-4002 (Luzchem, Ottawa, Canada) was used, with a spectral reading range of 230 to 900 nm.

Cytotoxicity assay

For cytotoxicity evaluation of the nanocomposite system constituted by CuO nanoparticles decorated on HAP/ferrite surface, *Allium cepa* L. seeds were used. *Allium cepa* L. seeds were initially selected and germinated in a Petri dish containing pure water at room temperature (± 25 °C). After the growth of the roots reached 1.5 to 2 cm in length, ten of them were separated and exposed with the suspension of CuO/HAP/ferrite at a concentration of 250 mg L^{-1} for 24 h, similar to the photocatalysis condition realized for RhB dye. A Carnoy's solution (3:1 (V/V) ethanol/acetic acid) was used in roots for 24 h, sequentially washed with water, and subjected to acid hydrolysis with a solution of 1 M HCl at 60 °C for 10 min. The samples were washed in distilled water and placed in contact with Schiff's reagent for 2 h in an amber glass bottle in a dark place. For removing the dye excedent, deionized water was used. The meristematic region was cut with a stainless steel blade and placed on a glass slide. For the analysis of the cellular alterations, slides were prepared being examined under an optical microscope. Additionally, a study of the Cu^{2+} ions released from the CuO-free nanoparticles and the nanocomposite was carried out to verify the composition stability. A PerkinElmer PinAAcle 900 T flame atomic absorption spectrophotometer (FAAS) was used to quantify the Cu^{2+} ions.

Bactericidal assay

Assays for the bactericidal effect evaluation were performed using diffusion disk methodology against *Staphylococcus aureus* (Gram-positive) and *Escherichia coli* (Gram-negative) in the presence of CuO-free nanoparticles and supported on the HAP/ferrite surface. Initially, the microorganisms were cultured in 10 mL of Mueller–Hinton broth culture medium (21 g L^{-1}) in a Falcon tube (15 mL) for 12 h at a temperature of 35.0 ± 0.5 °C. Then, the microorganism suspension was adjusted to 1 10^6 mL^{-1} cells using a Shimadzu UV-1601PC, UV–vis spectrophotometer at 625 nm, corresponding to the McFarland 0.5 standard. Next, a plate streak technique was essentially inoculated 100 µL of bacteria solution in a Petri dish containing Mueller–Hinton agar culture medium (30 mL solidified, 38 g L^{-1}). In the impregnated plaques, 5 mg of the samples was deposited in triplicate. After the inoculation period of 24 h at 35 °C ± 0.5, the inhibition halo was analyzed by observational analysis.

Results and discussion

X-ray diffraction was realized to evaluate the crystalline structure in a long and medium-range order of the interest compounds (XRD). Figure 1 shows the XRD patterns for the CuO monoclinic structure (JCPDS card nº 80–1268). Similarly, typical X-ray diffraction patterns were verified to monophasic spinel magnetite (JCPDS card nº 74–0748) and hexagonal HAP (JCPDS card n° 09–0432). As expected, HAP/ferrite support and CuO/HAP/ferrite nanocomposite presented characteristic peaks of pure HAP and ferrite. This fact indicates that the CuO nanoparticle decoration methodology was successfully applied to obtain a magnetic nanocomposite.

PL spectra have been shown as a sensitive tool (Paris et al. 2007; Gurgel et al. 2011; Oliveira et al. 2013). Figure 2 (a) shows the PL spectra of the pure HAP, ferrite, HAP/ferrite, and CuO/HAP/Ferrite samples excited at 325 nm wavelength with an argon-ion laser. Pure HAP sample emitted strong broadband centered at 507 nm due to the presence of thermally activated defects (André et al. 2012). Intermediate energy levels were confirmed as recombination events by decomposing the broadband spectrum into 3 Gaussian fits with 504, 445, and 572 nm centered peaks. However, the ferrite and respective compounds did not show luminescence spectra under these conditions, evidencing that ferrites promote HAP PL emission suppression. In Fig. 2b, Raman spectra were recorded at room temperature by exciting with

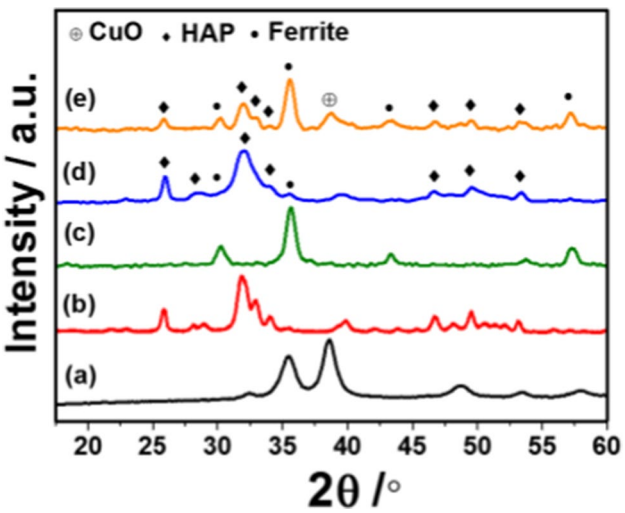

Fig. 1 X-ray diffraction patterns for (a) CuO, (b) HAP, (c) ferrite, (d) HAP/ferrite, and (e) CuO/HAP/ferrite samples

a 633 nm argon laser. Distinct HAP sample vibrational mode is verified at υ_1 961 cm^{-1} due to the PO_4^{3-} group in apatite structure (Yamini et al. 2014), observed for the HAP, HAP/ferrite, and CuO/HAP/ferrite samples. According to the literature (Wang et al. 2010), the CuO structure corresponds to the Cu_{2h}^6 space group and possesses three vibration modes. Thus, the active Raman optical phonons for the CuO sample observed A_g mode at 275 cm^{-1} and B_g at 330 cm^{-1}. Concerning HAP/ferrite and CuO/HAP/ferrite samples, characteristic modes in Fig. 2b confirm the ferrite presence in the composition. High-intense A1g modes located at approximately 669 cm^{-1} were observed in the ferrite sample and related to a crystalline structure disorder (Slavov et al. 2010). In contrast to high-intensity peaks, less intense peaks appear at 310 cm^{-1} and 530 cm^{-1} related to T_{1g} and E_g vibration modes (Shebanova and Lazor 2003). Therefore, the results suggest from Raman spectra (Fig. 2b) the presence of HAP, ferrite, and CuO in the short- and medium-range order in the final CuO/HAP/ferrite nanocomposite.

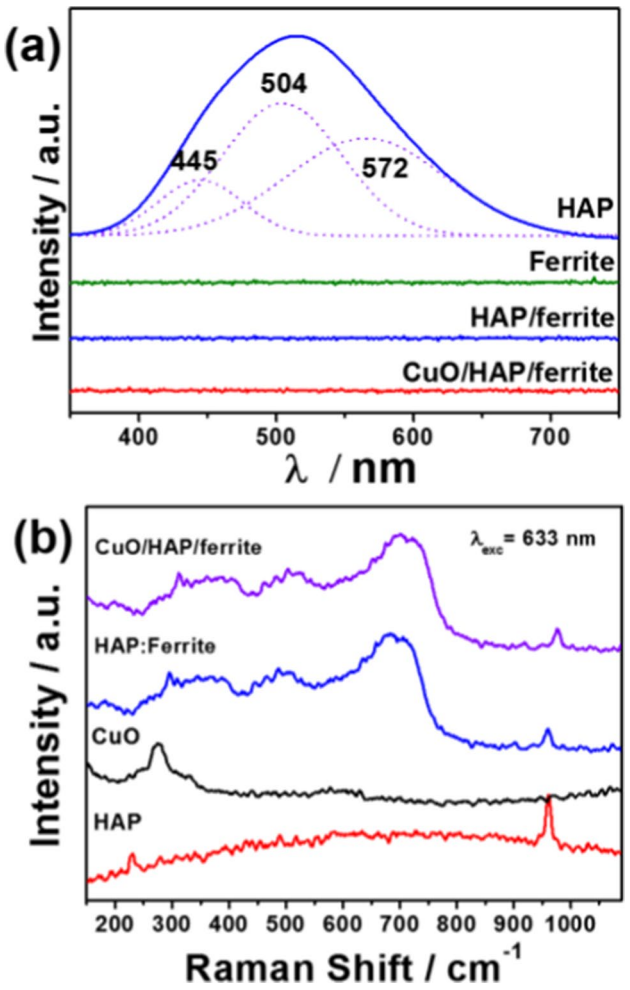

Fig. 2 Photoluminescence (a) and Raman spectra (b) of the HAP and CuO nanoparticles, HAP/ferrite magnetic support, and CuO/HAP/ferrite nanocomposite

Figure 3 shows the CuO-free nanoparticles and decorated on magnetic support morphology. As shown in CuO images (Fig. 3a), the nanoparticles possess an undefined form with a medium diameter of 10 ± 6 nm. The CuO/HAP/ferrite image (Fig. 3b) indicates particle sizes smaller than 25 nm for the system. EDS analysis showed that copper and iron elements were identified in CuO/HAP/ferrite. Figure 3c shows that the elemental compound mapping found Ca, P, Fe, and Cu evenly distributed, suggesting homogeneity in the sample. Four intense peaks are observed for Fe and Cu individually in the EDS spectrum (Fig. 3d). In comparison, less intensity two peaks are observed for each element, P and Ca, indicating the exciting elements in the CuO/HAP/ferrite nanocomposite.

XPS analyses were performed to characterize the surface chemical composition and electronic structure of CuO and CuO/HAP/ferrite samples. The survey and high-resolution XPS spectra are shown in Figs. 4 and 5, respectively. The results show that the CuO-free sample (Fig. 4a) has a surface composed mainly of Cu 2p (935.4 eV), Cu 3p (76.2 eV), and O 1 s (530.7 eV) assigned to the sample composition (Xu et al. 2016; Oruç and Altındal 2017). In Fig. 4b, in addition to the CuO peaks identified in Fig. 4a, the XPS survey spectrum showed P 2p (133.0 eV), Ca $2p_{3/2}$ (349.3 eV), Ca 2 s (437.6 eV), and Fe 2p (710.0 eV) signals (Nelson et al. 2002; Palanisamy et al. 2013; Xu et al. 2016), confirming that CuO/HAP/ferrite sample is composed for all expected elements. Furthermore, the observed C 1 s (286.4 eV) peak in both survey spectra could be related to adventitious carbon from the air contamination, the precursor acetate, or citric acid used in the synthesis procedures.

High-resolution XPS spectra of Cu, O, P, and Fe of CuO and CuO/HAP/ferrite samples are shown in Fig. 5. In Fig. 5a and b, Cu 2p XPS spectra show peaks centered at 933.6 and 941.4 eV, and 953.3 and 962.2 eV corresponding to $2p_{3/2}$ and $2p_{1/2}$ energy levels, respectively. These energy values are characteristic of Cu^{2+} and were observed for CuO and CuO/HAP/Fe_2O_3 samples (Xu et al. 2016). In Fig. 5c, the high-resolution XPS spectrum of O 1 s showed a peak centered at 530.0 eV and two shoulders centered at 531.4 and 533.1 eV. These binding energy values for the CuO sample are indexed to Cu–O, $Cu(OH)_2$, and O = C bonds, respectively (Oruç and Altındal 2017). For the CuO/HAP/ferrite sample, the high-resolution O 1 s spectrum shown in Fig. 5d is attributed to the O bonded with Cu, P, and Fe atoms due to the presence of HAP/ferrite support. Thus, the peaks centered at 530.0 eV are due to Cu–O/O-P bonding, 531.4 eV to Fe–O/C-O bonds, and 533.1 eV to C = O/C–OH bonds (Nelson et al. 2002; Lee et al. 2017). Figure 5e and f shows the high-resolution XPS spectra of Fe 2p, which presents binding energies at 710.8 and 724.8 eV, related to

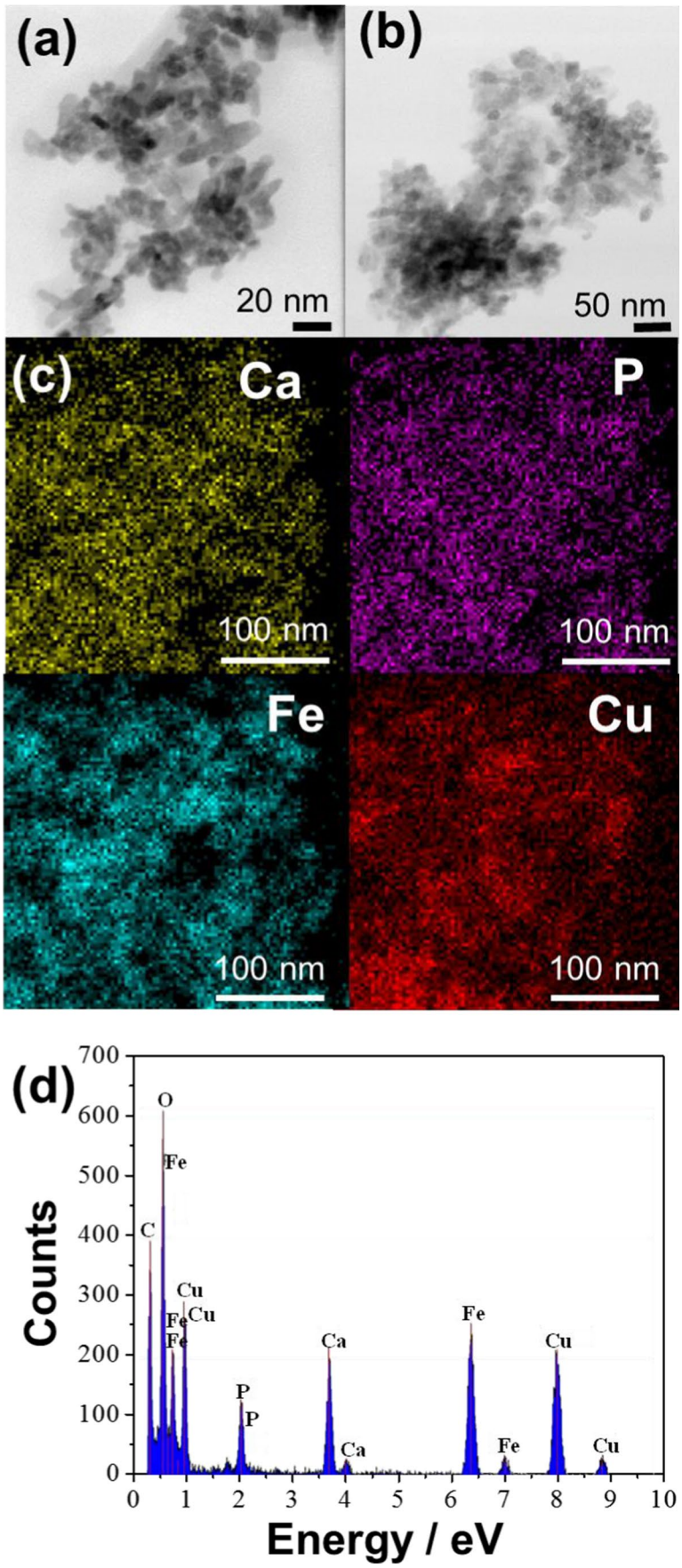

Fig. 3 TEM images of CuO-free nanoparticles (a) and (b) CuO/HAP/ferrite. EDS mapping (c) and spectrum for CuO-decorated on HAP/ferrite support (d)

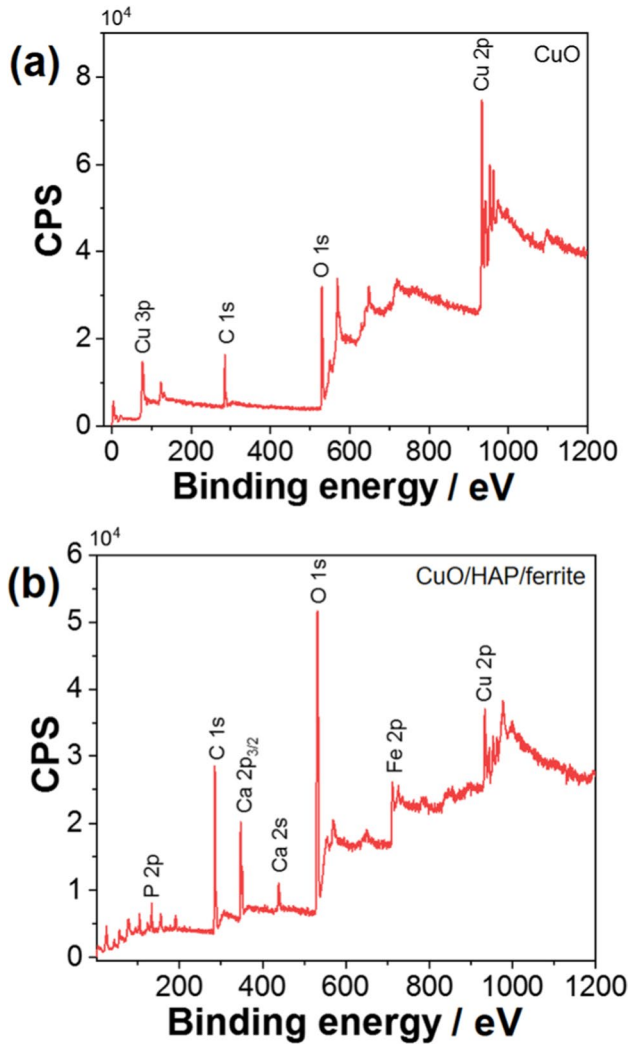

Fig. 4 XPS survey spectrum of CuO (a) and CuO/HAP/ferrite (b) samples

the energetic levels of Fe $2p_{3/2}$ and Fe $2p_{1/2}$, respectively, which are associated with Fe^{3+} (Yamashita and Hayes 2008). Finally, the P 2p XPS spectrum was deconvoluted in two peaks, the energy levels P $2p_{3/2}$ at 132.9 eV and P $2p_{1/2}$ at 133.9 eV, which are related to the P-O bond of HAP (Nelson et al. 2002). Therefore, XPS analysis proved that CuO/HAP/ferrite composite was successfully obtained using the synthesis route applied in this study.

Table 1 describes the zeta potential characterization of the CuO nanoparticles (+38.8 eV) with a positive charge; however, the ferrite sample showed a high negative charge (−43.0 eV). After HAP (−16.6 eV) insertion to HAP/ferrite support (−14.6 eV), the negative charge value decreased due to HAP's higher percentage on composition HAP/ferrite in the proportion of 3:1 (w/w). Also was observed a decrease in the negative charge value (−12.6 mV) for CuO/HAP/ferrite. This result can be attributed to the neutral charge surface of nanocomposite from the addition of CuO nanoparticles with a positive charge and the agglomeration effect. As an essential parameter in heterogeneous photocatalysis, the specific surface area (SSA) was measured and found 58.1 m^2g^{-1} for ferrite and 87.4 m^2g^{-1} for HAP. Due to magnetic properties and spin alignments, the ferrite nanoparticles tend to agglomerate even with a higher zeta potential, justifying the SSA value diminishing. As the HAP/ferrite support shows an SSA of 119.6 m^2g^{-1} higher than individual compounds, it is possible to affirm that the ferrite nanoparticles adhere to the HAP surface with good dispersion. Thus, the alignment of the spins in dried particles stabilizes the agglomeration of the magnetic material to increase the SSA values. Similarly, the nanocomposite CuO/HAP/ferrite (113.4 m^2g^{-1}) has a high SSA value, close to the support HAP/ferrite when decorated with CuO nanoparticles (77.2 m^2g^{-1}). Thus, HAP made it possible for the HAP/ferrite support to stabilize ferrites, increase the magnetic material surface area, and provide an adequate surface for impregnating CuO nanoparticles.

The magnetic hysteresis analysis was performed to investigate the magnetic response of the CuO and ferrite nanoparticles, support (HAP/ferrite), and nanocomposite (CuO/HAP/ferrite). Figure 4a and b illustrates the absence of magnetical property for the CuO nanoparticles, proving that ferrite nanoparticles provide the magnetic response in the CuO/HAP/ferrite. Figure 6a shows that the ferrite nanoparticles, HAP/ferrite, and CuO/HAP/ferrite presented saturation magnetization (Ms) with values 3.69, 3.40, and 2.78 emu g^{-1}, respectively. Thus, the support (HAP/ferrite) and the CuO/HAP/ferrite magnetic nanocomposite maintained the magnetic activity. This decrease concerning the pure magnetite sample values is due to the ferrite concentration reduction in these HAP/ferrite and CuO/HAP/ferrite compounds. Similar results were observed in the literature (Paris et al. 2020c) for cobalt ferrite immobilized on faujasite zeolite (1:3 w/w) evaluated for metallic ion adsorption.

CuO and ferrites absorb radiation with a wavelength in the visible region. Due to this characteristic, these materials are promising candidates for photocatalysis under visible light irradiation. Thus, diffuse reflectance measurements were performed. The bandgap energy (Egap) was calculated for CuO and CuO/HAP/ferrite. The results are shown in Fig. 7a for CuO, and CuO/HAP/ferrite, being found the values equal to 1.8 and 2.1 eV, respectively. Due to the high capacity of ferrites to absorb visible light, a similar bandgap value was found for CuO/HAP/ferrite nanocomposite (Paris et al. 2020c). However, CuO is a photocatalyst with activity in the visible light spectrum, giving CuO and CuO/HAP/ferrite evident photocatalytic potential to take advantage of light sources of lower energy and greater natural availability. Thus, for the photocatalytic assays, a fluorescent lamp with visible emission was chosen. The emission spectra of the

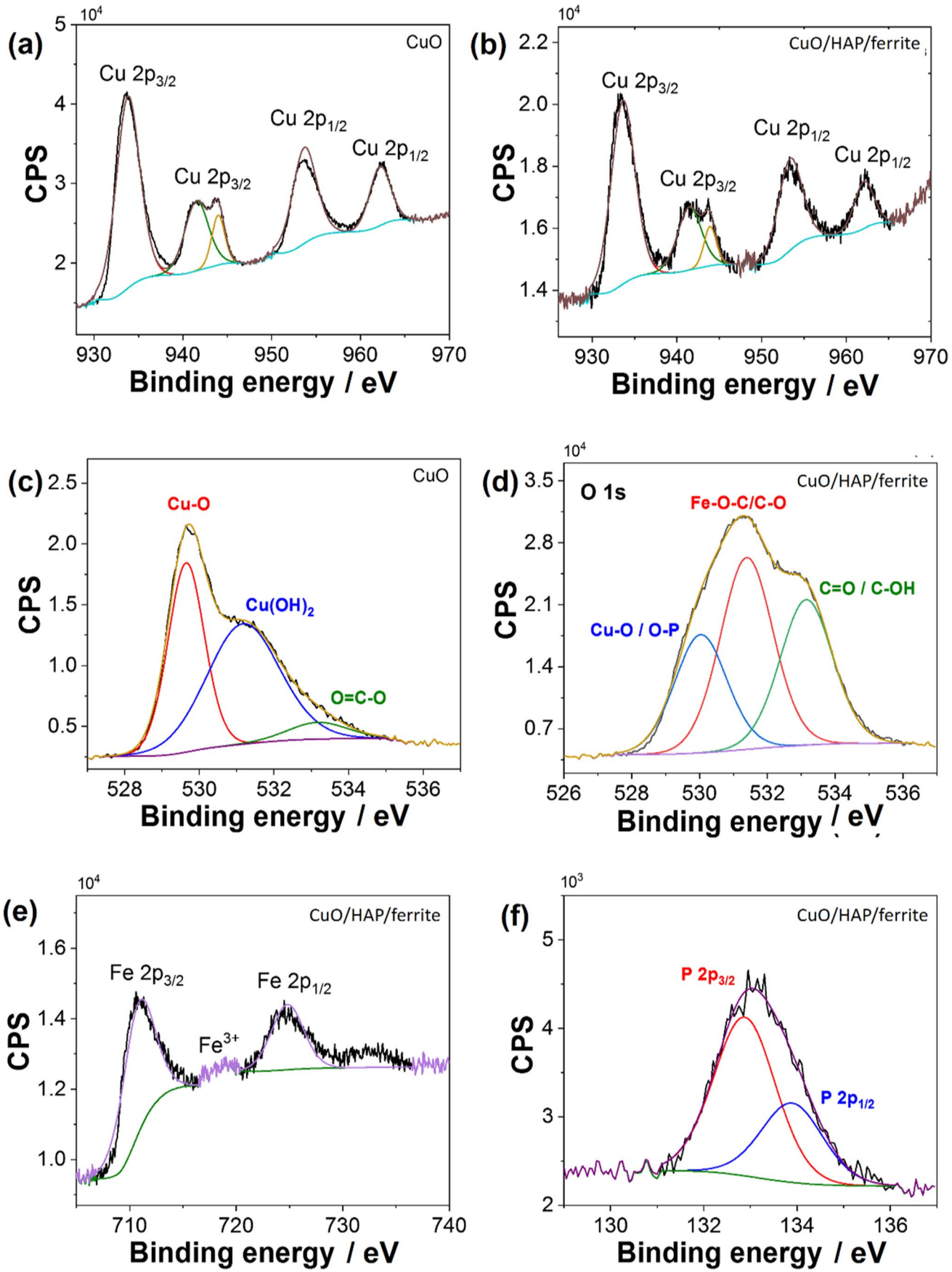
(a)
CuO
Cu 2p3/2
Cu 2p3/2
Cu 2p1/2
Cu 2p1/2
CPS
Binding energy / eV
(b)
CuO/HAP/ferrite
Cu 2p3/2
Cu 2p3/2
Cu 2p1/2
Cu 2p1/2
CPS
Binding energy / eV
(c)
CuO
Cu-O
Cu(OH)2
O=C-O
CPS
Binding energy / eV
(d)
O 1s
CuO/HAP/ferrite
Fe-O-C/C-O
C=O / C-OH
Cu-O / O-P
CPS
Binding energy / eV
(e)
CuO/HAP/ferrite
Fe 2p3/2
Fe 2p1/2
Fe3+
CPS
Binding energy / eV
(f)
CuO/HAP/ferrite
P 2p3/2
P 2p1/2
CPS
Binding energy / eV

◂**Fig. 5** High-resolution XPS spectrum of Cu, O, P, and Fe elements for the CuO and CuO/HAP/ferrite samples

light source are shown in Fig. 7b. A wide-band spectrum is noted between regions 366 and 750 nm, with low-intensity peaks which are identified in the UV-A regions (366 to 407 nm). In comparison, more intense peaks are noted above 437 nm.

After the characterization analysis and selection of the appropriate light source, the color removal assay using CuO-free nanoparticles was used to evaluate the nanocomposite ability in the environmental remediation of organic compounds. Figure 8a shows the photodegradation for RhB under visible radiation in the presence of CuO nanoparticles with different H_2O_2 volumes from 0.1 to 2 mL to verify the influence for $^{\bullet}OH$ production. Since H_2O_2 addition equal to 1 mL was not observed significant increment in photodegradation behavior (in the range from 90 to 95% removal) by superior volumes. In this way, the H_2O_2 volume of 1 mL was fixed for the photocatalytic assays. As the CuO photocatalytic activity was highlighted in the H_2O_2 presence, its performance can be attributed to a synergistic effect, which allows the oxidizing species formation in solution and promotes the organic compound oxidation (Moreira et al. 2020a).

Furthermore, H_2O_2 aid in inhibiting the electron pair recombination since it interacts with the CuO electrons in the conduction band to generate $^{\bullet}OH$ (Zhang et al. 2014). Subsequently, the increase in CuO concentration response in gain during the photocatalytic activity was evaluated. As shown in Fig. 8b, a thrice increase of the CuO concentration (50 to 150 mg L^{-1}) did not cause a significant variation on RhB degrading, maintenance about 95% removal. Thus, the lowest CuO concentration evaluated was sufficient to remove RhB dye kinetic constant (k) value correspondent $k = 0.050 \pm 0.006$ min^{-1}.

Once that RhB dye photodegradation optimized conditions by CuO-free were elucidated, the photocatalytic test was performed for the magnetic nanocomposite. For this purpose, 250 mg L^{-1} of the magnetic compound was used to guarantee 50 mg L^{-1} for CuO nanoparticles in CuO/HAP/ferrite nanocomposite in the photocatalytic system. Figure 9 shows the efficacy of the photodegradation process from 90 to 95%, verifying a similar activity to CuO-free nanoparticles. Nezamzadeh-Ejhieh and Hushmandrad (2010) synthesized a material composed of zeolite and CuO to evaluate the photocatalytic activity under sunlight with 94% of color removal after 3 h of photodegradation. After applying the recovery with a neodymium magnet from the aqueous medium, the CuO/HAP/ferrite showed the same efficiency after the 3rd cycle, maintaining the photocatalytic activity. Thus, the CuO/HAP/ferrite magnetic nanocomposites showed similar efficiency compared to CuO-free nanoparticles. Also, the recovered photocatalyst promised photocatalytic activity preservation after 3 consecutive cycles.

Therefore, the results show no significant change in the 3 initial application cycles, indicating the absence of poisoning of the photocatalyst active sites. The kinetic constants of CuO/HAP/ferrite nanocomposite in all cycles were similar with values about $k = 0.01 \pm 0.01$ min^{-1}, being inferior compared to CuO-free nanoparticles due to the lower CuO surface area in the photocatalytic system. To clarify the photocatalytic mechanism of CuO and CuO/HAP/ferrite during RhB degradation, $^{\bullet}OH$ probe assays are shown in Fig. 9b. In the $^{\bullet}OH$ presence, COU is oxidized to form umbelliferone, presenting PL emission with a peak centered at 542 nm after excitation at 342 nm (Malafatti et al. 2020; Moreira et al. 2020b). As shown in Fig. 9b, the photolysis (visible + H_2O_2) cannot form significant $^{\bullet}OH$ amounts, and, therefore, RhB degradation was not evidenced (Fig. 8). However, two intense peaks of umbelliferone are noted when the photocatalytic process is carried out in the presence of CuO and CuO/HAP/ferrite, confirming that $^{\bullet}OH$ are the reactive species formed in the photocatalytic process under visible irradiation. The greater intensity of PL emission verified for CuO shows that this material promotes the photocatalytic reduction of H_2O_2 to form $^{\bullet}OH$, while the decrease in intensity verified for CuO/HAP/ferrite is the consequence of the loss surface area due to the immobilization. These results corroborate CuO's slightly higher photocatalytic activity, confirming that this semiconductor is directly responsible for the degradation mechanism, which was represented by the set of Eqs. 1 to 7 (Ghashghaee et al. 2019).

RhB mechanism degradation in h^+ (VB):

$$CuO + hv(visible) \rightarrow h + (VB) + e^{-}CB) \quad (1)$$

$$h^+(VB) + H_2O_2 \rightarrow HO_2^{\bullet} + H^+ \quad (2)$$

$$HO_2^{\bullet} \rightarrow O_2^{\bullet} + H^+ \quad (3)$$

$$O_2^{\bullet} + RhB \rightarrow \text{degradation products} \quad (4)$$

RhB mechanism degradation in e^- (CB):

$$CuO + hv(visible) \rightarrow h^+(VB) + e^-(CB) \quad (5)$$

$$e^-(CB) + H_2O_2 \rightarrow HO^{\bullet} + OH^- \quad (6)$$

$$HO^{\bullet} + RhB \rightarrow \text{degradation products} \quad (7)$$

In addition to the photocatalytic application, the CuO/HAP/ferrite compound cytotoxic response was analyzed at a 250 mg L^{-1} concentration (equivalent to the photocatalytic test) in the *Allium cepa* roots during the cell mitosis

Table 1 Values of zeta potential and physisorption/desorption by the BET method

Sample	Surface area/$m^2\ g^{-1}$	Zeta potential/mV
CuO	77.2	+38.8
HAP	87.4	−16.6
Ferrite	58.1	−43.0
HAP/ferrite	119.6	−14.2
CuO/HAP/ferrite	113.4	−12.6

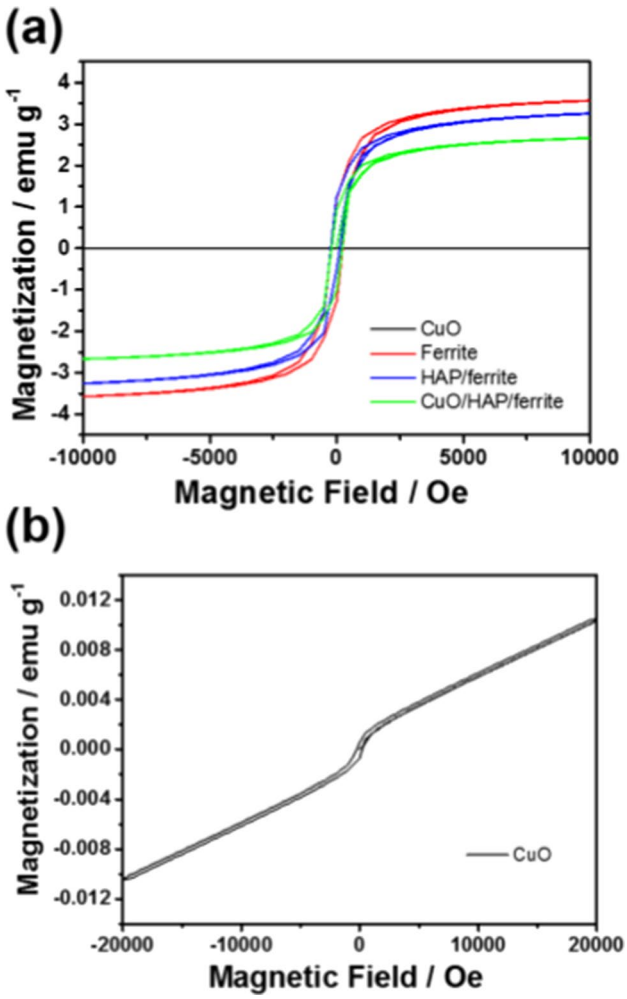

Fig. 6 Magnetic hysteresis for the CuO and ferrite nanoparticles, HAP/ferrite support, and CuO/HAP/ferrite nanocomposite

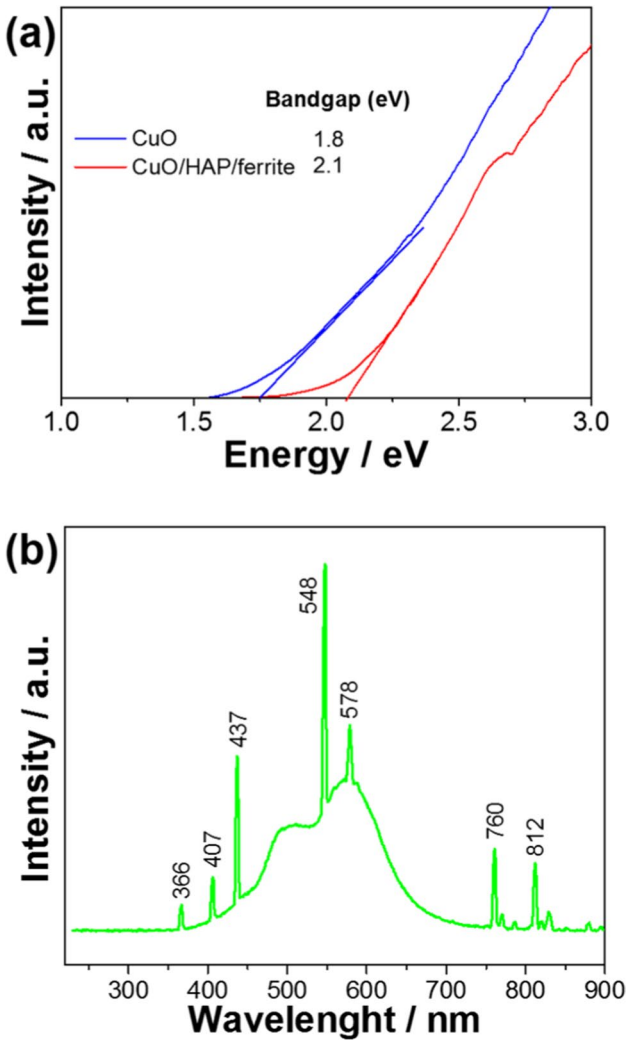

Fig. 7 DRS spectra for the CuO and CuO/HAP/ferrite *nano*composite (a) and emission light source (b)

processes. Figure 10 indicates that most of the cells showed an expected and intact behavior. However, in the cell meristem was verified common mutations during the cell division stage. This result can be attributed to the interaction between nanoparticles and cell metabolism in live organisms (Leme and Marin-Morales 2009). According to Hou et al. (Hou et al. 2017), CuO nanoparticles can act on plant and animal cells through CuO endocytosis and the permeation of Cu^{2+} ions through the channels present in the plasma membrane. The authors explain that the harmful effects are exploited with the increase in particle concentration and increased solubilization. The central mechanism of cellular toxicity is oxidative stress derived from highly reactive •OH (Cronholm et al. 2013).

Due to oxidative stress, the main aberration types found in cells are regular meristem alterations (prophase, metaphase, anaphase, and telophase). Figure 10 shows some abnormalities caused by contact with the CuO/HAP/ferrite compound, which occurred in a few punctual cells. These abnormalities were the appearance of chromosomal bridge telophase (Fig. 10a), cytoplasmic bridges (Fig. 10b), and interphase with micronucleus appearance (Fig. 8c) that are commonly found in *Allium cepa* strain cells exposed to different compounds, such as CuO (Deng et al. 2016). In addition, Cu^{2+} ions are also known to promote inhibition

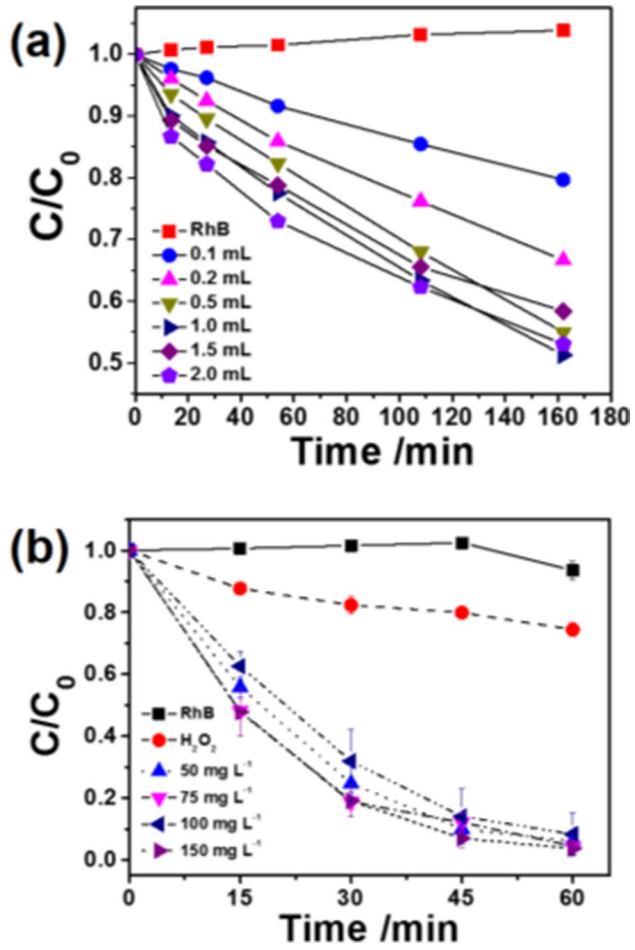

Fig. 8 Photocatalytic activity with 50 mg L^{-1} of CuO nanoparticles in different H_2O_2 concentrations (a) and variation of CuO concentration in 1 mL of H_2O_2 (b)

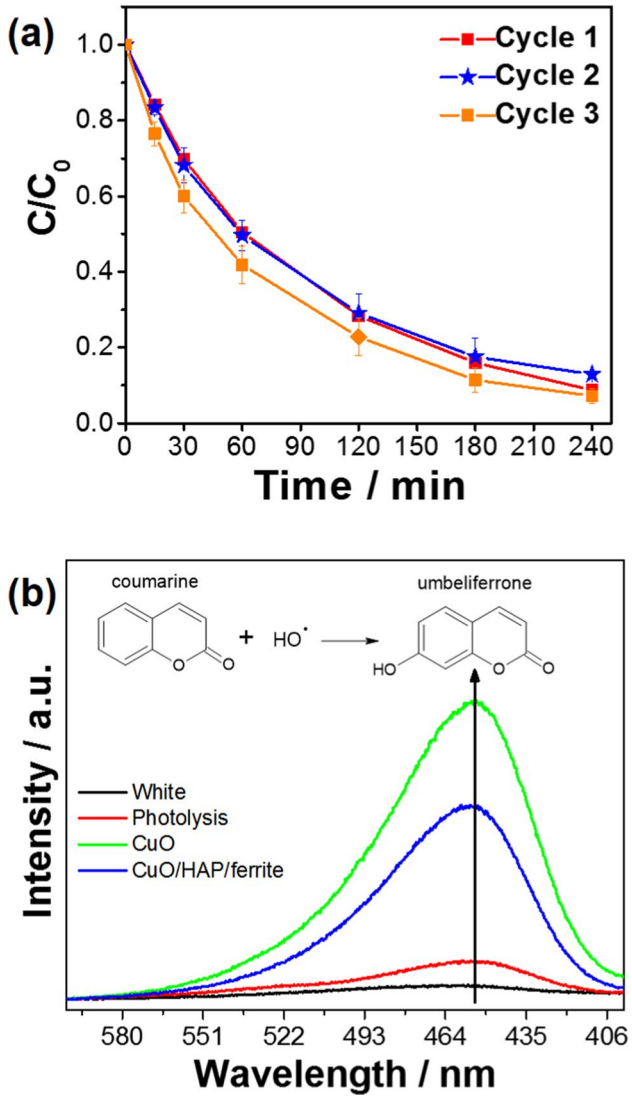

Fig. 9 Reuse evaluation of the CuO/HAP/ferrite nanocomposite for RhB photocatalysis with 0.5 mL of H_2O_2 (a) and $^{\bullet}OH$ probe assays by COU reaction to form the photoluminescent umbelliferone product (b)

of seed germination and microbial activity due to oxidative stress caused in environmental systems (Ochoa-Herrera et al. 2011; Smiri and Missaoui 2014). The final solutions obtained after 4 h of photocatalytic process in the presence of CuO and CuO/HAP/ferrite found a concentration of Cu^{2+} leached of 0.15 and 0.05 mg L^{-1}, respectively. These concentrations are deficient compared to the proven toxicity for different species when the Cu^{2+} concentration was 0.95 mg L^{-1} (Ochoa-Herrera et al. 2011). Therefore, the low concentration of Cu^{2+} ions leached corroborates with low toxicity to cells that remained intact after exposure to the CuO/HAP/ferrite system, indicating a minimum environmental impact on plants in the ecosystem.

As CuO-based materials also have antimicrobial properties, bactericidal disk diffusion assays were performed against *S. aureus* and *E. coli* microorganisms (Fig. 11). The results show CuO-free nanoparticles with a positive antimicrobial activity for both bacteria. The appearance of diameter inhibition in *S. aureus* (Gram-positive) and *E. coli* (Gram-negative) indicates activity for different bacteria groups. As shown in Fig. 11, the response was better for *S. aureus* (0.83 ± 0.02 cm) than *E. coli* (0.54 ± 0.03 cm). This result can be attributed to the structural differences in the membranes of Gram-positive and Gram-negative bacteria. Gram-positive bacteria (*S. aureus*) have many carboxyl and hydroxyl groups on the outer membrane surface, which have an affinity for CuO (Rincón Joya et al. 2019).

In contrast, Gram-negative bacteria such as *E. coli* have a cell wall on the outer membrane surface, which increases resistance to interaction and the passage of antimicrobial agents such as CuO nanoparticles. No bactericidal activity was observed for the HAP/ferrite magnetic support (Fig. 10) due to the absence of inhibition diameter in the

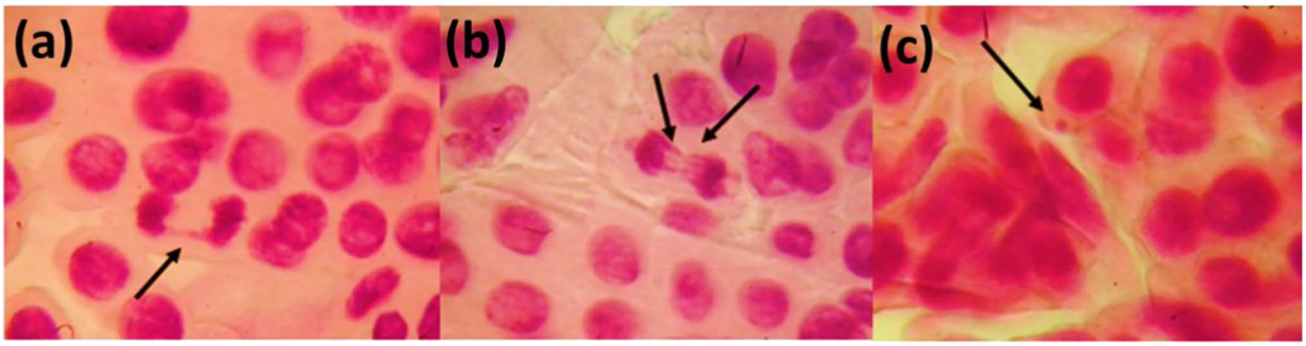

Fig. 10 Cytotoxic response for *Allium cepa* cells with 250 mg L^{-1} of CuO/HAP/ferrite nanocomposite: (a) typical aberrations, (b) telophase with chromosomal and cytoplasmic bridges, and (c) interphase with micronucleus appearance

same microorganisms. However, when HAP/ferrite support is decorated with CuO nanoparticles is verified the appearance of an inhibition halo in *S. aureus* (0.47 ± 0.03 cm). Thus, it is observed that the CuO nanoparticles promote the bactericidal activity of the nanocomposite.

Rajabi et al. (2016) obtained magnetite support with mordenite zeolite to anchor CuO nanoparticles, being observed similar result, evidencing the activity of the antimicrobial agent from the CuO nanoparticles. According to the authors, the antimicrobial activity from the composite material was due to the Cu^{2+} ion release, which allows interaction with the bacterial membrane. However, the physiological environment has a negative charge due to the carboxyl, hydroxyl, and phosphate groups present on the surface of lipoproteins. Therefore, the CuO-free nanoparticles have abbreviated bactericidal activity with immobilization as CuO/HAP/ferrite nanocomposite system due to the reduced active surface area; however, the response for Gram-positive bacteria stayed efficient. Thus, the CuO/HAP/ferrite system showed an excellent candidate to control the *S. aureus* bacteria with easy magnetical remotion after the water remediation process.

Conclusions

According to the results, ferrite, HAP, and CuO obtaining methodologies were efficient, allowing the synthesis of nanometric and monophasic particles. A HAP/ferrite magnetic support with homogeneous CuO nanoparticle distribution was obtained, maintaining the magnetic properties for the nanocomposite photocatalyst. The $^{\bullet}OH$ radical prove assays confirmed that CuO is responsible for H_2O oxidation to generate $^{\bullet}OH$ for RhB dye oxidizing. The CuO-decorated on the magnetic support provided a high efficiency of the photocatalytic process maintenance with color removal of 90% up to 1 h of exposure to visible radiation. The photocatalyst was recovered by applying a magnet and remained active for reuse in three photocatalytic degradation cycles. From *Allium cepa* germination assays, the photocatalyst

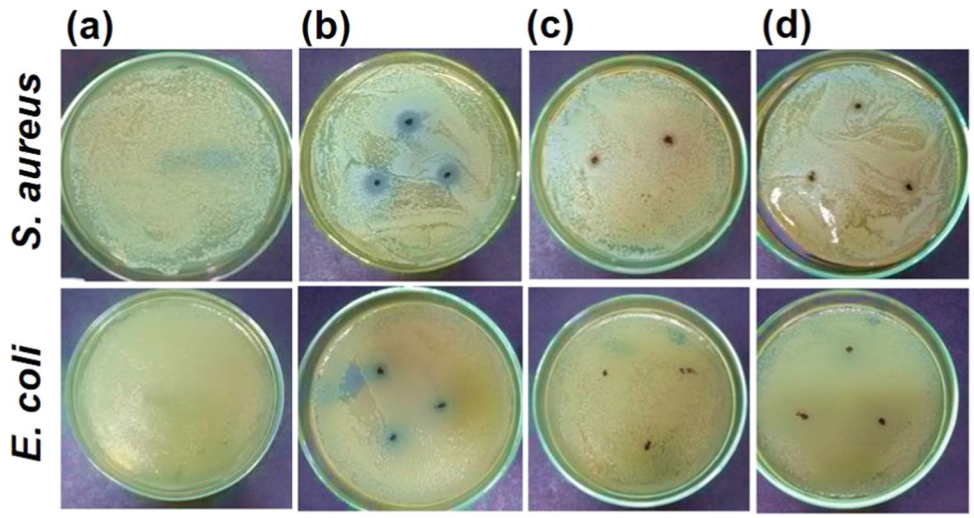

Fig. 11 (a) Bactericidal effect of CuO-free, HAP/ferrite support, and CuO/HAP/ferrite nanocomposite against *S. aureus* and *E. coli* microorganisms

environmental toxicity response did not indicate significance at 250 mg L^{-1} by meristematic cell tissue analysis. Furthermore, CuO nanoparticles supported on HAP/ferrite showed an efficient bactericidal activity for *S. aureus* bacteria (Gram-positive). Thus, the HAP/ferrite nanocomposite decorated by CuO showed an excellent candidate for water remediation, acting like a complete and easy recovery system for the treatment due to achievement in critical points, including organic contaminant degradation and bacteria control without significant cytotoxicity to the ecosystem.

Acknowledgements The authors acknowledge CAPES (001 Code), Embrapa (grant no. 03.14.03.002.00.00, 21.14.03.001.03.00), CNPq (grant no. 311440/2014-2), FINEP, SisNano, and AgroNano Network for financial support and professors M. S. Li and P. S. Pizani for photoluminescence and Raman measurements, respectively.

Author contribution Elaine Cristina Paris: Writing, conceptualization, supervision, review, and editing. João Otávio Donizette Malafatti: Writing, review, and editing. Ailton José Moreira: Methodology, writing, review, and editing. Lílian Cruz Santos: Methodology. Camila Rodrigues Sciena: Methodology. Alessandra Zenatti: Methodology. Márcia Tsuyama Escote: Methodology. Valmor Roberto Mastelaro: Methodology, writing, review, and editing. Miryam Rincón Joya: Writing, review, and editing.

Availability of data and materials The datasets used and/or analyzed during the current study are available from the corresponding author on reasonable request.

Declarations

Ethics approval and consent to participate Not applicable.

Consent for publication Not applicable.

Competing interests The authors declare no competing interests.

References

Ahamed M, Alhadlaq HA, Khan MAM et al (2014) Synthesis, characterization, and antimicrobial activity of copper oxide nanoparticles. J Nanomater 2014:1–4. https://doi.org/10.1155/2014/637858

Ain QU, Zhang H, Yaseen M et al (2020) Facile fabrication of hydroxyapatite-magnetite-bentonite composite for efficient adsorption of Pb(II), Cd(II), and crystal violet from aqueous solution. J Clean Prod 247:119088. https://doi.org/10.1016/j.jclepro.2019.119088

André RS, Paris EC, Gurgel MFC et al (2012) Structural evolution of Eu-doped hydroxyapatite nanorods monitored by photoluminescence emission. J Alloys Compd 531:50–54. https://doi.org/10.1016/j.jallcom.2012.02.053

Augusto TM, Chagas P, Sangiorge DL et al (2018) Iron ore tailings as catalysts for oxidation of the drug paracetamol and dyes by heterogeneous Fenton. J Environ Chem Eng 6:6545–6553. https://doi.org/10.1016/j.jece.2018.09.052

Bordbar M, Sharifi-Zarchi Z, Khodadadi B (2017) Green synthesis of copper oxide nanoparticles/clinoptilolite using Rheum palmatum L. root extract: high catalytic activity for reduction of 4-nitro phenol, rhodamine B, and methylene blue. J Sol-Gel Sci Technol 81:724–733. https://doi.org/10.1007/s10971-016-4239-1

Coutinho TC, Rojas MJ, Tardioli PW et al (2018) Nanoimmobilization of β-glucosidase onto hydroxyapatite. Int J Biol Macromol 119:1042–1051. https://doi.org/10.1016/j.ijbiomac.2018.08.042

Cronholm P, Karlsson HL, Hedberg J et al (2013) Intracellular uptake and toxicity of Ag and CuO nanoparticles: a comparison between nanoparticles and their corresponding metal ions. Small 9:970–982. https://doi.org/10.1002/smll.201201069

Deng F, Wang S, Xin H (2016) Toxicity of CuO nanoparticles to structure and metabolic activity of Allium cepa root tips. Bull Environ Contam Toxicol 97:702–708. https://doi.org/10.1007/s00128-016-1934-0

Dong C, Xiao X, Chen G et al (2015) Morphology control of porous CuO by surfactant using combustion method. Appl Surf Sci 349:844–848. https://doi.org/10.1016/j.apsusc.2015.04.149

Gallo A, Manfra L, Boni R et al (2018) Cytotoxicity and genotoxicity of CuO nanoparticles in sea urchin spermatozoa through oxidative stress. Environ Int 118:325–333. https://doi.org/10.1016/j.envint.2018.05.034

Ghashghaee M, Fallah M, Rabiee A (2019) Superhydrophobic nanocomposite coatings of poly(methyl methacrylate) and stearic acid grafted CuO nanoparticles with photocatalytic activity. Prog Org Coatings 136. https://doi.org/10.1016/j.porgcoat.2019.105270

Gurgel MF, Moreira ML, Paris EC et al (2011) BaZrO3 photoluminescence property: an ab initio analysis of structural deformation and symmetry changes. Int J Quantum Chem 111:694–701. https://doi.org/10.1002/qua

Hamzezadeh-Nakhjavani S, Tavakoli O, Akhlaghi SP et al (2015) Efficient photocatalytic degradation of organic pollutants by magnetically recoverable nitrogen-doped TiO2 nanocomposite photocatalysts under visible light irradiation. Environ Sci Pollut Res 22:18859–18873. https://doi.org/10.1007/s11356-015-5032-3

Harraz FA, Mohamed RM, Rashad MM et al (2014) Magnetic nanocomposite based on titania-silica/cobalt ferrite for photocatalytic degradation of methylene blue dye. Ceram Int 40:375–384. https://doi.org/10.1016/j.ceramint.2013.06.012

Hou J, Wang X, Hayat T, Wang X (2017) Ecotoxicological effects and mechanism of CuO nanoparticles to individual organisms. Environ Pollut 221:209–217. https://doi.org/10.1016/j.envpol.2016.11.066

Hu W, Yuan X, Liu X et al (2017) Hierarchical SnO2 nanostructures as high efficient photocatalysts for the degradation of organic dyes. J Sol-Gel Sci Technol 84:316–322. https://doi.org/10.1007/s10971-017-4511-z

Jiang T, Wang Y, Meng D et al (2014) Controllable fabrication of CuO nanostructure by hydrothermal method and its properties. Appl Surf Sci 311:602–608. https://doi.org/10.1016/j.apsusc.2014.05.116

Lee D, Kwon OS, Song SH (2017) Tailoring the performance of magnetic elastomers containing Fe2O3 decorated carbon nanofiber. RSC Adv 7:45595–45600. https://doi.org/10.1039/c7ra08861b

Leme DM, Marin-Morales MA (2009) Allium cepa test in environmental monitoring: a review on its application. Mutat Res - Rev Mutat Res 682:71–81. https://doi.org/10.1016/j.mrrev.2009.06.002

Li D, Tang Y, Ao D et al (2019) Ultra-highly sensitive and selective H2S gas sensor based on CuO with sub-ppb detection limit. Int J Hydrogen Energy 44:3985–3992. https://doi.org/10.1016/j.ijhydene.2018.12.083

Mageshwari K, Sathyamoorthy R, Park J (2015) Photocatalytic activity of hierarchical CuO microspheres synthesized by facile reflux condensation method. Powder Technol 278:150–156. https://doi.org/10.1016/j.powtec.2015.03.004

Malafatti JOD, Moreira AJ, Sciena CR et al (2020) Prozac® removal promoted by HAP:Nb2O5 nanoparticles system: by products,

mechanism, and cytotoxicity assessment. J Environ Chem Eng 9. https://doi.org/10.1016/j.jece.2020.104820
Meshram SP, Adhyapak PV, Mulik UP, Amalnerkar DP (2012) Facile synthesis of CuO nanomorphs and their morphology dependent sunlight driven photocatalytic properties. Chem Eng J 204–205:158–168. https://doi.org/10.1016/j.cej.2012.07.012
Moreira AJ, Campos LO, Maldi CP et al (2020a) Photocatalytic degradation of Prozac® mediated by TiO2 nanoparticles obtained via three synthesis methods: sonochemical, microwave hydrothermal, and polymeric precursor. Environ Sci Pollut Res. https://doi.org/10.1007/s11356-020-08798-x
Moreira AJ, Malafatti JOD, Giraldi TR et al (2020b) Prozac® photodegradation mediated by Mn-doped TiO2 nanoparticles: evaluation of by-products and mechanisms proposal. J Environ Chem Eng 8. https://doi.org/10.1016/j.jece.2020.104543
Moura AP, Cavalcante LS, Sczancoski JC et al (2010) Structure and growth mechanism of CuO plates obtained by microwave-hydrothermal without surfactants. Adv Powder Technol 21:197–202. https://doi.org/10.1016/j.apt.2009.11.007
Nelson AE, Hildebrand NKS, Major PW (2002) Mature dental enamel [calcium hydroxyapatite, Ca10(PO4)6(OH)2] by XPS. Surf Sci Spectra 9:250–259. https://doi.org/10.1116/11.20030701
Nezamzadeh-Ejhieh A, Hushmandrad S (2010) Solar photodecolorization of methylene blue by CuO/X zeolite as a heterogeneous catalyst. Appl Catal A Gen 388:149–159. https://doi.org/10.1016/j.apcata.2010.08.042
Nolting F, Scholl A, Stöhr J et al (2000) Direct observation of the alignment of ferromagnetic spins by antiferromagnetic spins. Nature 405:767–769. https://doi.org/10.1038/35015515
Novikova AA, Moiseeva DY, Karyukov EV, Kalinichenko AA (2016) Facile preparation photocatalytically active CuO plate-like nanoparticles from brochantite. Mater Lett 167:165–169. https://doi.org/10.1016/j.matlet.2015.12.157
Ochoa-Herrera V, León G, Banihani Q et al (2011) Toxicity of copper(II) ions to microorganisms in biological wastewater treatment systems. Sci Total Environ 412–413:380–385. https://doi.org/10.1016/j.scitotenv.2011.09.072
Oliveira LH, Paris EC, Avansi W et al (2013) Correlation between photoluminescence and structural defects in Ca1+xCu3-XTi4O12 systems. J Am Ceram Soc 96:209–217. https://doi.org/10.1111/jace.12020
Oruç Ç, Altındal A (2017) Structural and dielectric properties of CuO nanoparticles. Ceram Int 43:10708–10714. https://doi.org/10.1016/j.ceramint.2017.05.006
Osman AI, Abu-Dahrieh JK, Rooney DW et al (2017) Surface hydrophobicity and acidity effect on alumina catalyst in catalytic methanol dehydration reaction. J Chem Technol Biotechnol 92:2952–2962. https://doi.org/10.1002/jctb.5371
Osman AI, Skillen NC, Robertson PKJ et al (2020) Exploring the photocatalytic hydrogen production potential of titania doped with alumina derived from foil waste. Int J Hydrogen Energy 45:34494–34502. https://doi.org/10.1016/j.ijhydene.2020.02.065
Palanisamy B, Babu CM, Sundaravel B et al (2013) Sol–gel synthesis of mesoporous mixed Fe2O3/TiO2 photocatalyst: application for degradation of 4-chloropheno. J Hazard Mater 252–253:233–242. https://doi.org/10.1016/j.jhazmat.2013.02.060
Paris EC, Espinosa JWM, de Lazaro S et al (2007) Er3+ as marker for order-disorder determination in the PbTiO3 system. Chem Phys 335:7–14. https://doi.org/10.1016/j.chemphys.2007.03.019
Paris EC, Malafatti JOD, Musetti HC et al (2020a) Faujasite zeolite decorated with cobalt ferrite nanoparticles for improving removal and reuse in Pb2+ ions adsorption. Chinese J Chem Eng. https://doi.org/10.1016/j.cjche.2020.04.019
Paris EC, Malafatti JOD, Musetti HC et al (2020b) Faujasite zeolite decorated with cobalt ferrite nanoparticles for improving removal and reuse in Pb2+ ions adsorption. Chinese J Chem Eng 28:1884–1890. https://doi.org/10.1016/j.cjche.2020.04.019
Paris EC, Malafatti JOD, Sciena CR et al (2020c) Nb2O5 nanoparticles decorated with magnetic ferrites for wastewater photocatalytic remediation. Environ Sci Pollut Res. https://doi.org/10.1007/s11356-020-11262-5
Pedrosa M, Pastrana-Martínez LM, Pereira MFR et al (2018) N/S-doped graphene derivatives and TiO2 for catalytic ozonation and photocatalysis of water pollutants. Chem Eng J 348:888–897. https://doi.org/10.1016/j.cej.2018.04.214
Pereira FF, Paris EC, Bresolin JD et al (2017) Investigation of nanotoxicological effects of nanostructured hydroxyapatite to microalgae Pseudokirchneriella subcapitata. Ecotoxicol Environ Saf 144:138–147. https://doi.org/10.1016/j.ecoenv.2017.06.008
Phiwdang K, Suphankij S, Mekprasart W, Pecharapa W (2013) Synthesis of CuO nanoparticles by precipitation method using different precursors. Energy Procedia 34:740–745. https://doi.org/10.1016/j.egypro.2013.06.808
Raba-Páez AM, João JO, Parra-Vargas CA et al (2020a) Structural evolution, optical properties, and photocatalytic performance of copper and tungsten heterostructure materials. Mater Today Commun 26. https://doi.org/10.1016/j.mtcomm.2020.101886
Raba-Páez AM, Malafatti JOD, Parra-Vargas CA et al (2020b) Effect of tungsten doping on the structural, morphological and bactericidal properties of nanostructured CuO. PLoS ONE 15. https://doi.org/10.1371/journal.pone.0239868
Rajabi SK, Sohrabnezhad S, Ghafourian S (2016) Fabrication of Fe3O4@CuO core-shell from MOF based materials and its antibacterial activity. J Solid State Chem 244:160–163. https://doi.org/10.1016/j.jssc.2016.09.034
Rana S, Jonnalagadda SB (2017) CuO/graphene oxide nanocomposite as highly active and durable catalyst for selective oxidation of cyclohexane. ChemistrySelect 2:2277–2281. https://doi.org/10.1002/slct.201601637
Rincón Joya M, Barba Ortega J, Malafatti JOD, Paris EC (2019) Evaluation of photocatalytic activity in water pollutants and cytotoxic response of α-Fe2O3 nanoparticles. ACS Omega 4:17477–17486. https://doi.org/10.1021/acsomega.9b02251
Ruellas TMO, Peçanha LOO, Domingos GHS et al (2019) Zinc oxide pieces obtained by pressing and slip casting: physical, structural and photocatalytic properties. Environ Technol (united Kingdom). https://doi.org/10.1080/09593330.2019.1683078
Sharma K, Dutta V, Sharma S et al (2019) Recent advances in enhanced photocatalytic activity of bismuth oxyhalides for efficient photocatalysis of organic pollutants in water: a review. J Ind Eng Chem 78:1–20. https://doi.org/10.1016/j.jiec.2019.06.022
Shebanova ON, Lazor P (2003) Raman study of magnetite (Fe3O4): laser-induced thermal effects and oxidation. J Raman Spectrosc 34:845–852. https://doi.org/10.1002/jrs.1056
Shinde DR, Tambade PS, Chaskar MG, Gadave KM (2017) Photocatalytic degradation of dyes in water by analytical reagent grade photocatalysts – a comparative study. Drink Water Eng Sci Discuss 1–16. https://doi.org/10.5194/dwes-2017-20
Slavov L, Abrashev MV, Merodiiska T et al (2010) Raman spectroscopy investigation of magnetite nanoparticles in ferrofluids. J Magn Magn Mater 322:1904–1911. https://doi.org/10.1016/j.jmmm.2010.01.005
Smiri M, Missaoui T (2014) The role of ferredoxin: THioredoxin reductase/thioredoxin m in seed germination and the connection between this system and copper ion toxicity. J Plant Physiol 171:1664–1670. https://doi.org/10.1016/j.jplph.2014.06.019
Tavakoli A, Hashemzadeh MS (2020) Inhibition of herpes simplex virus type 1 by copper oxide nanoparticles. J Virol Methods 275:113688–113694. https://doi.org/10.1016/j.jviromet.2019.113688

Tu SH, Wu HC, Wu CJ et al (2014) Growing hydrophobicity on a smooth copper oxide thin film at room temperature and reversible wettability transition. Appl Surf Sci 316:88–92. https://doi.org/10.1016/j.apsusc.2014.07.183

Usha V, Kalyanaraman S, Thangavel R, Vettumperumal R (2015) Effect of catalysts on the synthesis of CuO nanoparticles: structural and optical properties by sol-gel method. Superlattices Microstruct 86:203–210. https://doi.org/10.1016/j.spmi.2015.07.053

Valizadeh S, Rasoulifard MH, Seyed Dorraji MS (2014) Modified Fe3O4- hydroxyapatite nanocomposites as heterogeneous catalysts in three UV, Vis and Fenton like degradation system. Appl Surf Sci 319:358–366. https://doi.org/10.1016/j.apsusc.2014.07.139

Wang LP, Yu L, Satish R et al (2014) High-performance hybrid electrochemical capacitor with binder-free Nb2O5@graphene. RSC Adv 4:37389. https://doi.org/10.1039/C4RA06674J

Wang W, Zhou Q, Fei X et al (2010) Synthesis of CuO nano- and micro-structures and their Raman spectroscopic studies. CrystEngComm 12:2232–2237. https://doi.org/10.1039/b919043k

Xiang JY, Tu JP, Zhang L et al (2010) Simple synthesis of surface-modified hierarchical copper oxide spheres with needle-like morphology as anode for lithium ion batteries. Electrochim Acta 55:1820–1824. https://doi.org/10.1016/j.electacta.2009.10.073

Xu ZX, Xu GS, Fu XQ, Wang Q (2016) The mechanism of nano-CuO and CuFe2o4 catalyzed thermal decomposition of ammonium nitrate. Nanomater Nanotechnol 6:1–10. https://doi.org/10.1177/1847980416681699

Xue X, yan, Cheng R, Shi L, et al (2017) Nanomaterials for water pollution monitoring and remediation. Environ Chem Lett 15:23–27. https://doi.org/10.1007/s10311-016-0595-x

Yamashita T, Hayes P (2008) Analysis of XPS spectra of Fe2+ and Fe3+ ions in oxide materials. Appl Surf Sci 254:2441–2449. https://doi.org/10.1016/j.apsusc.2007.09.063

Yamini D, Devanand Venkatasubbu G, Kumar J, Ramakrishnan V (2014) Raman scattering studies on PEG functionalized hydroxyapatite nanoparticles. Spectrochim Acta - Part A Mol Biomol Spectrosc 117:299–303. https://doi.org/10.1016/j.saa.2013.07.064

Yang S, Zhang C, Cai Y et al (2018) Synthesis of CdxZn1−xS@Fe3S4 magnetic photocatalyst nanoparticles for the photodegradation of methylene blue. J Alloys Compd 735:1955–1961. https://doi.org/10.1016/j.jallcom.2017.11.301

Yang Z, Gong X, Zhang C (2010) Recyclable Fe 3 O 4 / hydroxyapatite composite nanoparticles for photocatalytic applications. Chem Eng J 165:117–121. https://doi.org/10.1016/j.cej.2010.09.001

Zhang YF, Qiu LG, Yuan YP et al (2014) Magnetic Fe3O4@C/Cu and Fe3O4@CuO core-shell composites constructed from MOF-based materials and their photocatalytic properties under visible light. Appl Catal B Environ 144:863–869. https://doi.org/10.1016/j.apcatb.2013.08.019

Zhao F, Zou Y, Lv X et al (2015) Synthesis of CoFe2O4-zeolite materials and application to the adsorption of gallium and indium. J Chem Eng Data 60:1338–1344. https://doi.org/10.1021/je501039u

Zhu J, Bi H, Wang Y et al (2008) CuO nanocrystals with controllable shapes grown from solution without any surfactants. Mater Chem Phys 109:34–38. https://doi.org/10.1016/j.matchemphys.2007.10.027